

LHC AND LEPTON FLAVOUR VIOLATION PHENOMENOLOGY IN SEESAW MODELS

J. C. ROMÃO

*Departamento de Física & CFTP, Instituto Superior Técnico, Technical University of Lisbon
A. Rovisco Pais 1, 1049-001 Lisboa, Portugal*

We review Lepton Flavour Violation (LFV) in the supersymmetric version of the seesaw mechanism (type I, II, III) and in Left-Right models. The LFV needed to explain neutrino masses and mixings is the only source of LFV and has experimental implications both in low-energy experiments where we search for the radiative decays of leptons, and at the LHC where we look at its imprint on the LFV decays of the sparticles and on slepton mass splittings. We discuss how this confrontation between high- and low-energy LFV observables may provide information about the underlying mechanism of LFV.

1 Introduction

The experimental observation of non-vanishing neutrino masses and mixings,¹ constitutes clear evidence for physics beyond the Standard Model (SM). As neutrino oscillations indisputably signal lepton flavour violation (LFV) in the neutral sector, it is only natural to expect that charged lepton flavour will also be violated in extensions of the SM where ν oscillations can be naturally accommodated. The search for manifestations of charged LFV constitutes the goal of several experiments,² exclusively dedicated to look for signals of processes such as rare radiative as well as three-body decays and lepton conversion in muonic nuclei.

In parallel to these low-energy searches, if the high-energy Large Hadron Collider (LHC) finds signatures of supersymmetry (SUSY), it is then extremely appealing to consider SUSY models that can also accommodate neutrino oscillations. One of the most economical and elegant possibilities is perhaps to embed a seesaw mechanism in this framework, the so-called SUSY seesaw.

If the seesaw is indeed the source of both neutrino masses and leptonic mixings and accounts for low-energy LFV observables within future sensitivity reach, we show that interesting phenomena are expected to be observed at the LHC: in addition to measurable slepton mass splittings, the most striking effect will be the possible appearance of new edges in di-lepton mass distributions.

2 Models

2.1 Seesaw type I, II, III & Left-Right Model

At GUT scale the SU(5) invariant superpotentials for type I, II and III SUSY seesaw are³

$$W_{\text{RHN}} = \mathbf{Y}_N^I N^c \bar{5} \cdot 5_H + \frac{1}{2} M_R N^c N^c, \quad (1)$$

$$W_{15H} = \frac{1}{\sqrt{2}} \mathbf{Y}_N^{II} \bar{5} \cdot 15 \cdot \bar{5} + \frac{1}{\sqrt{2}} \lambda_1 \bar{5}_H \cdot 15 \cdot \bar{5}_H + \frac{1}{\sqrt{2}} \lambda_2 5_H \cdot \bar{15} \cdot 5_H + \mathbf{Y}_5 10 \cdot \bar{5} \cdot \bar{5}_H$$

$$+ \mathbf{Y}_{10} 10 \cdot 10 \cdot 5_H + M_{15} 15 \cdot \overline{15} + M_5 \overline{5}_H \cdot 5_H , \quad (2)$$

$$W_{24H} = \sqrt{2} \overline{5}_M Y^5 10_M \overline{5}_H - \frac{1}{4} 10_M Y^{10} 10_M 5_H + 5_H 24_M Y_N^{III} \overline{5}_M + \frac{1}{2} 24_M M_{24} 24_M . \quad (3)$$

The exchange of the singlet N^c in type I, of the scalar triplet T in type II and of both the

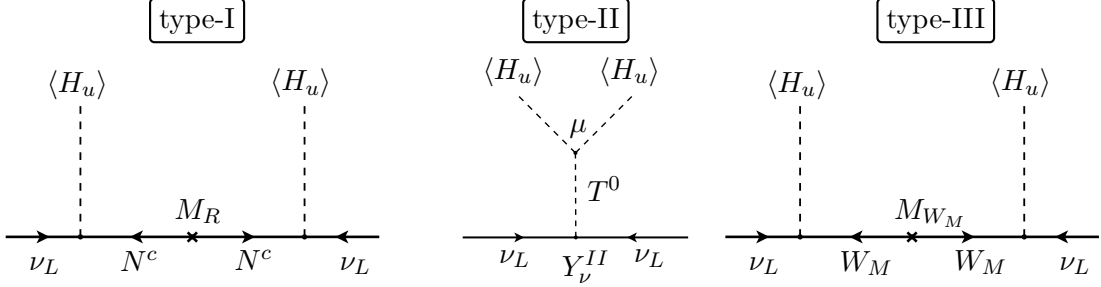


Figure 1: Seesaw types

fermionic triplet W_M and fermionic singlet B_M in type III lead, through the diagrams of Fig. 1 to the well known effective neutrino mass matrix formulas,

$$m_{\text{eff}}^{\text{I}} = -(vY_\nu)M_R^{-1}(vY_\nu)^T, \quad m_{\text{eff}}^{\text{II}} = \frac{v^2 \mu Y_\nu^{\text{II}}}{M_T^2}, \quad m_{\text{eff}}^{\text{III}} = -(vY_\nu^{\text{III}})M_{W_M}^{-1}(vY_\nu^{\text{III}})^T . \quad (4)$$

We have also studied⁴ a SUSY seesaw in which the breaking from $SU(5)$ to the SM gauge group is done in two steps, first to a Left-Right (LR) symmetric model, $SU(3)_c \times SU(2)_L \times SU(2)_R \times U(1)_{B-L}$ at scale v_R , and then with the $B-L$ broken at a lower scale v_{B-L} . For neutrino physics, as well as for the LFV, the relevant part of the superpotential is,

$$\mathcal{W}^{LR} = Y_L L \Phi L^c - f_c L^c \Delta^c L^c + \dots , \quad (5)$$

where Y_L and f_c complex 3×3 matrices. After the $B-L$ breaking we have,

$$\mathcal{L} = H_u \overline{\nu}_L Y_\nu^{\text{I}} \nu_R - \frac{1}{2} \nu_R^T C^{-1} (f_c v_{BL}) \nu_R + \dots , \quad (6)$$

leading to an effective neutrino mass matrix of the type I form,

$$m_{\text{eff}}^{\text{LR}} = -(vY_\nu)(f_c v_{BL})^{-1}(vY_\nu)^T . \quad (7)$$

The important point here is that, as we have two complex matrices, we can have different types of neutrino fits. We studied two limiting situations, the so-called Y_ν fit where $f_c = \mathbf{1}$ (Y_ν arbitrary), and the f fit where $Y_\nu = \mathbf{1}$ (f_c arbitrary). These will leave different imprints on the LFV through their RGE running.

2.2 LFV in the Models

Starting with universal minimal supergravity inspired (mSUGRA) boundary conditions at M_{GUT} , the off-diagonal entries in Y^ν will induce the LFV on the slepton mass matrices through RGE effects. For type I, II and III we have

$$\Delta m_{L,ij}^2 \simeq -\frac{a_k}{8\pi^2} (3m_0^2 + A_0^2) \left(Y_N^{k,\dagger} L Y_N^k \right)_{ij} , \quad L = \ln\left(\frac{M_{\text{GUT}}}{M_N}\right) \quad (8)$$

$$\Delta m_{E,ij}^2 \simeq 0 \quad a_{\text{I}} = 1 , \quad a_{\text{II}} = 6 \quad \text{and} \quad a_{\text{III}} = \frac{9}{5} , \quad (9)$$

while for the LR model we have two situations. From M_{GUT} to v_R ,

$$\Delta m_L^2 \simeq -\frac{1}{4\pi^2} \left(3ff^\dagger + Y_L^{(k)} Y_L^{(k)\dagger} \right) (3m_0^2 + A_0^2) \ln \left(\frac{M_{\text{GUT}}}{v_R} \right) \quad (10)$$

$$\Delta m_E^2 \simeq -\frac{1}{4\pi^2} \left(3f^\dagger f + Y_L^{(k)\dagger} Y_L^{(k)} \right) (3m_0^2 + A_0^2) \ln \left(\frac{M_{\text{GUT}}}{v_R} \right), \quad (11)$$

while from v_R to v_{BL} ,

$$\Delta m_L^2 \simeq -\frac{1}{8\pi^2} Y_\nu Y_\nu^\dagger (m_L^2|_{v_R} + A_e^2|_{v_R}) \ln \left(\frac{v_R}{v_{BL}} \right), \quad \Delta m_E^2 \simeq 0. \quad (12)$$

Therefore, the choice of the different neutrino fits will have implications on the lepton flavour violation observables. The low energy LFV processes are described by an effective Lagrangian,

$$\mathcal{L}_{eff} = e \frac{m_{l_i}}{2} \bar{l}_i \sigma_{\mu\nu} F^{\mu\nu} (A_L^{ij} P_L + A_R^{ij} P_R) l_j + h.c. \quad (13)$$

For seesaw models,

$$A_L^{ij} \sim \frac{(\Delta m_L^2)_{ij}}{m_{\text{SUSY}}^4}, \quad A_R^{ij} \sim \frac{(\Delta m_E^2)_{ij}}{m_{\text{SUSY}}^4}. \quad (14)$$

This implies that for type I, II and III we have only $A_L \neq 0$, while for the LR model we can have both, A_L and A_R . This implies that if MEG² finds evidence for the decay $\mu^+ \rightarrow e^+ \gamma$, then we can distinguish among the models by looking at the positron polarization asymmetry,

$$\mathcal{A}(\mu^+ \rightarrow e^+ \gamma) = \frac{|A_L|^2 - |A_R|^2}{|A_L|^2 + |A_R|^2} \begin{cases} = 1 & \text{type-I-II-III} \\ \neq 1 & \text{LR} \end{cases}. \quad (15)$$

3 Results

For all the models we have studied^{3,4,5} the different low- and high-energy LFV observables. The numerical analysis was done using the public code SPheno,⁶ that includes the 2-loop RGEs calculated with the public code SARAH.⁷

3.1 Low-Energy Observables

The present bounds on low-energy LFV observables and dark matter abundance already constrain the parameter space of the models. As an example we give in Fig. 2 the type II case. On the left panel we show the allowed regions for dark matter abundance (within 3σ of the WMAP⁸ observation). A scan was performed in the $M_{1/2} - m_0$ plane, the other cMSSM parameters being taken as $A_0 = 0$, $\tan\beta = 10$, $\mu > 0$. The seesaw scale was fixed at $M_T = 5 \times 10^{13}$ GeV. Superimposed are the contours for $\text{BR}(\mu \rightarrow e\gamma)$. We see that for these input parameters only a small part of the parameter space remains viable after imposing the LFV and dark matter constrains. Once MEG gets to the sensitivity of 10^{-13} , most of the parameter space will be excluded if no signal is found. On the right panel of Fig. 2 we show a similar plot, now in the so-called Higgs funnel region obtained for $\tan\beta = 52$, the other parameters as before. The variation with the top mass is shown: $m_{top} = 169.1$ GeV (blue), 171.2 GeV (red), 173.3 GeV (green).

As another example we consider the e^+ asymmetry defined in Eq. (15) in the LR model⁴. On the left panel of Fig. 3 we show the contours for \mathcal{A} in the $M_{1/2} - m_0$ plane. The cMSSM parameters were taken as those of the SPS3 point, $m_0 = 90$ GeV, $M_{1/2} = 400$ GeV, $A_0 = 0$ GeV, $\tan\beta = 10$ and $\mu > 0$. We take $M_{\text{Seesaw}} = 10^{12}$ GeV, while the LR breaking scales were $v_{BL} = 10^{15}$ GeV, $v_R \in [10^{14}, 10^{15}]$ GeV and Y_ν fit was chosen. On the right panel we show, for the same parameters, the correlation between the asymmetry and the breaking scales. If MEG measures $\mathcal{A} < 1$, we can have an handle on the scales v_R, v_{BL} and test the LR model.

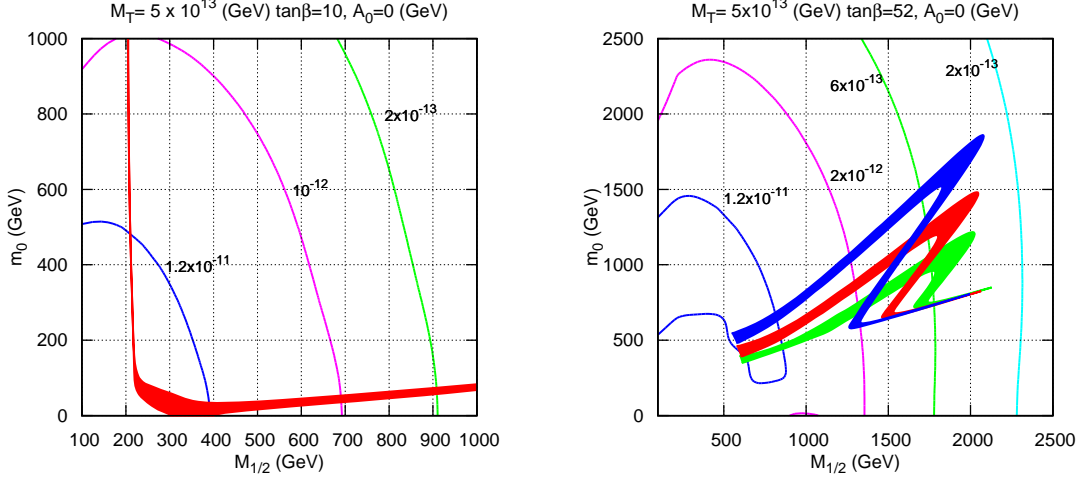


Figure 2: Dark matter allowed regions and $\text{BR}(\mu \rightarrow e\gamma)$ contours for type II,

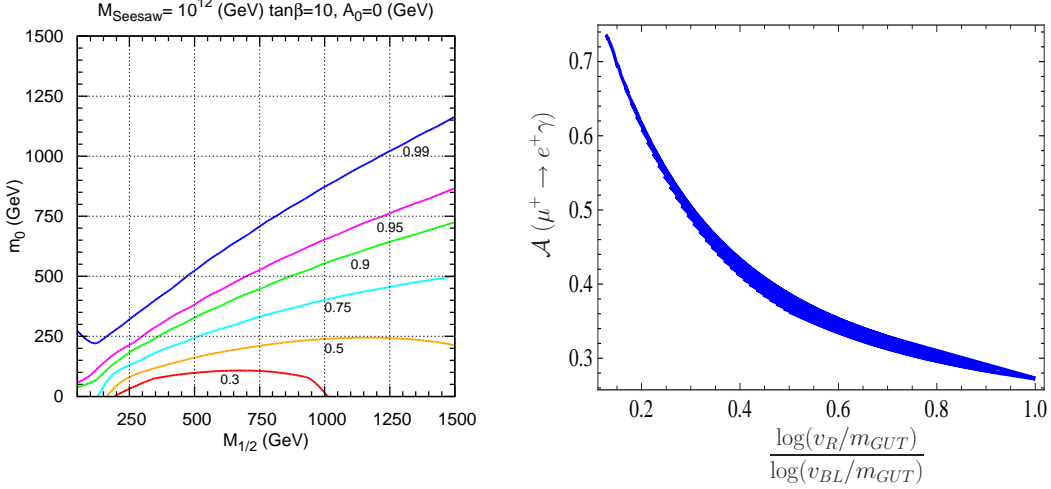


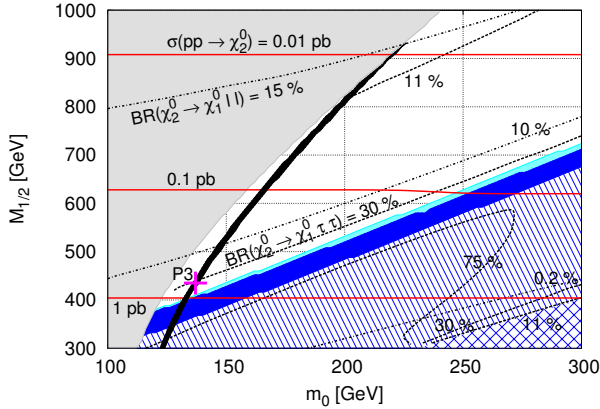
Figure 3: Positron asymmetry in the Left-Right model.

3.2 LHC Observables

At LHC we look at di-lepton invariant mass distributions from $\chi_2^0 \rightarrow \tilde{\ell}_{L,R}^i \ell \rightarrow \chi_1^0 \ell \ell$ decays, that can be measured with a precision of 0.1%,⁹ for on-shell sleptons and isolated leptons with large $p_T > 10$ GeV. From this we can infer the slepton mass splittings,

$$\frac{\Delta m_{\tilde{\ell}}}{m_{\tilde{\ell}}}(\tilde{\ell}_i, \tilde{\ell}_j) = \frac{|m_{\tilde{\ell}_i} - m_{\tilde{\ell}_j}|}{\langle m_{\tilde{\ell}_{i,j}} \rangle} \quad @\text{LHC} : \begin{cases} \Delta m/m_{\tilde{\ell}}(\tilde{e}_L, \tilde{\mu}_L) \sim \mathcal{O}(0.1\%) \\ \Delta m/m_{\tilde{\ell}}(\tilde{\mu}_L, \tilde{\tau}_L) \sim \mathcal{O}(1\%) \end{cases} \quad (16)$$

We start our analysis by identifying what we call a *standard window*. This is defined by the requirement of having on-shell sleptons decaying with isolated leptons with large $p_T > 10$ GeV. We also require large χ_2^0 production, a sizable $\text{BR}(\chi_2^0 \rightarrow \chi_1^0 \ell \ell)$ and, if possible, the correct abundance of dark matter, Ωh^2 . This is shown on the left panel of Fig. 4, where the white region fulfills all the requirements (the correct dark matter abundance corresponds to the black line inside the region). To carry out our analysis we chose the cMSSM study points shown in the right panel of Fig. 4 and then varied the seesaw parameters. In the cMSSM we get double-triangular distributions corresponding to intermediate $\tilde{\mu}_L$ and $\tilde{\mu}_R$ in $\chi_2^0 \rightarrow \chi_1^0 \mu \mu$, with superimposed $\tilde{\ell}_{L,R}$ edges for $m_{\mu\mu}$ and m_{ee} because of “degenerate” $\tilde{\mu}, \tilde{e}$. In Fig. 5 we show the di-muon invariant distribution, and number of expected events, for the case of SUSY type



Point	m_0 (GeV)	$M_{1/2}$ (GeV)	A_0 (TeV)	$\tan \beta$
P1	110	528	0	10
P2	110	471	1	10
P3	137	435	-1	10
P4	490	1161	0	40
P5-HM1	180	850	0	10
P6-SU1	70	350	0	10

Figure 4: Standard window (see text) and benchmark points used in the analysis.

I seesaw, for the following choice of seesaw parameters: $M_N = \{10^{10}, 5 \times 10^{10}, 5 \times 10^{13}\}$ GeV (P2', P3') and $M_N = \{10^{10}, 5 \times 10^{12}, 10^{15}\}$ GeV (P1''', SU1'''), always with $\theta_{13} = 0.1^\circ$. We get

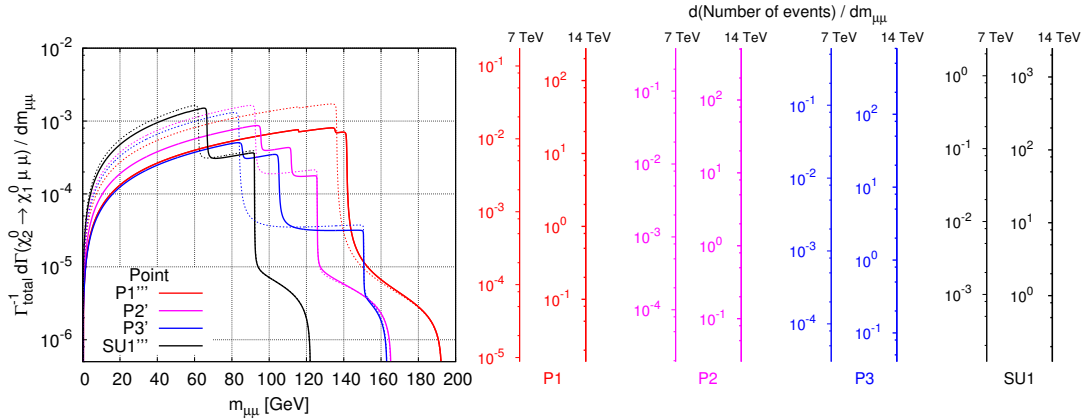


Figure 5: Di-muon invariant mass distribution for the SUSY seesaw for the benchmark points defined in Fig. 4.

displaced $m_{\mu\mu}$ and m_{ee} edges (ℓ_L) which give sizable mass splittings $\frac{\Delta m_{\tilde{\ell}}}{m_{\tilde{\ell}}}(\tilde{e}_L, \tilde{\mu}_L)$. We also find the appearance of a new edge in $m_{\mu\mu}$ corresponding to an intermediate $\tilde{\tau}_2$. These mass splittings are correlated with the low-energy observables as we show in Fig. 6. On the left panel we show the correlation for $\text{BR}(\mu \rightarrow e\gamma)$ for the CMS benchmark point HM1 ($m_0 = 180$ GeV, $M_{1/2} = 800$ GeV, $A_0 = 0$ GeV, $\tan \beta = 10$ and $\mu > 0$) while on the right panel we show the correlation for $\text{BR}(\tau \rightarrow \mu\gamma)$ for the ATLAS benchmark point SU1 ($m_0 = 70$ GeV, $M_{1/2} = 350$ GeV, $A_0 = 0$ GeV, $\tan \beta = 10$ and $\mu > 0$). In these plots we performed a scan over the SUSY seesaw parameters, with $M_{N_3} = 10^{12,13,14}$ GeV, $\theta_{13} = 0.1^\circ$.

We conclude that if SUSY is discovered with a spectrum similar to HM1 or SU1 and a type-I seesaw is at work, then the LFV observables will be within experimental reach at LHC, while $\text{BR}(\mu \rightarrow e\gamma)$ and $\text{BR}(\tau \rightarrow e\gamma)$ will be within the reach of MEG and SuperB, respectively.

4 Conclusions

In SUSY seesaw models the neutrino Yukawa couplings, Y_ν , acts as the only source of LFV, implying a correlation between low- and high-energy LFV observables. We have performed a study of these correlations in the so-called SUSY seesaws type I, II and III, as well as in a seesaw model that is Left-Right symmetric below the GUT scale.

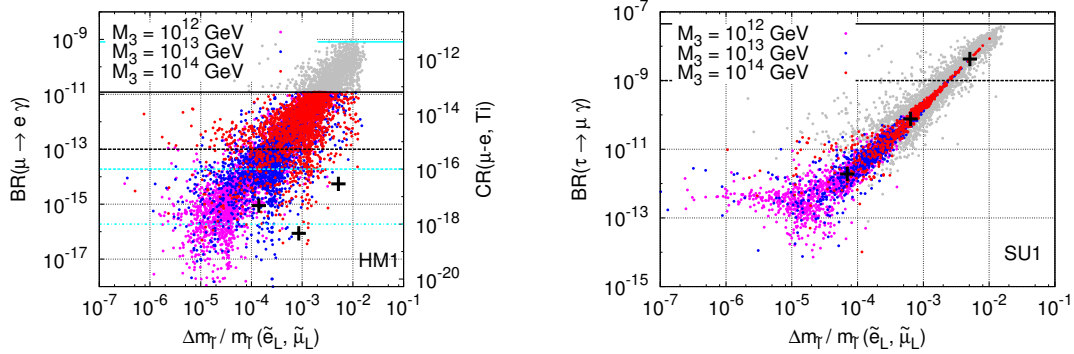


Figure 6: Correlation between low-energy and LHC observables for the benchmark points HM1 and SU1.

If SUSY seesaw is to account for neutrino masses and mixings then we will have slepton mass splittings within LHC sensitivity, with the possible observation of new edges in the di-lepton invariant mass distributions. In most cases a clear correlation can be established between low- and high-energy LFV observables (e.g. BR vs $\Delta m_{\tilde{\ell}}$) due to their unique source.

The experimental data that will be available soon, both from the high- and low-energy experiments, will either substantiate the seesaw hypothesis, or disfavour the SUSY seesaw as the (only) source of flavour violation.

Acknowledgments

This work has been done partly under the EU Network grant UNILHC PITN-GA-2009-237920 and from *Fundação para a Ciência e a Tecnologia* grants CFTP-FCT UNIT 777, PTDC/FIS/102120/2008, CERN/FP/109305/2009.

References

1. For a recent review see T. Schwetz, M. Tortola, J. W. F. Valle, [arXiv:1103.0734 [hep-ph]].
2. For a comprehensive list see Ref. ⁵.
3. M. Hirsch, J. W. F. Valle, W. Porod, J. C. Romao and A. Villanova del Moral, Phys. Rev. D **78** (2008) 013006; J. N. Esteves, J. C. Romao, A. Villanova del Moral, M. Hirsch, J. W. F. Valle and W. Porod, JHEP **0905**, 003 (2009); J. N. Esteves, J. C. Romao, M. Hirsch, F. Staub and W. Porod, Phys. Rev. D **83** (2011) 013003.
4. J. N. Esteves, J. C. Romao, M. Hirsch, A. Vicente, W. Porod, F. Staub, JHEP **1012** (2010) 077.
5. A. Abada, A. J. R. Figueiredo, J. C. Romao and A. M. Teixeira, JHEP **1010** (2010) 104; *ibidem* [arXiv:1104.3962 [hep-ph]].
6. W. Porod, Comput. Phys. Commun. **153**, (2003) 275.
7. F. Staub, Comput. Phys. Commun. **181** (2010) 1077-1086.
8. D. Larson *et al.*, Astrophys. J. Suppl. **192** (2011) 16.
9. F. E. Paige, "Determining SUSY particle masses at LHC", arXiv:hep-ph/9609373; I. Hinchliffe, F. E. Paige, M. D. Shapiro, J. Soderqvist and W. Yao, Phys. Rev. D **55** (1997) 5520; H. Bachacou, I. Hinchliffe and F. E. Paige, Phys. Rev. D **62** (2000) 015009.